



# Controlled Nanoconfinement of Polyimide Networks in Mesoporous $\gamma$ -Alumina Membranes for the Molecular Separation of Organic Dyes

Nikos Kyriakou, Louis Winnubst, Martin Drobek, Sissi de Beer, Arian Nijmeijer, Alix Pizzoccaro-Zilamy

## ► To cite this version:

Nikos Kyriakou, Louis Winnubst, Martin Drobek, Sissi de Beer, Arian Nijmeijer, et al.. Controlled Nanoconfinement of Polyimide Networks in Mesoporous  $\gamma$ -Alumina Membranes for the Molecular Separation of Organic Dyes. ACS Applied Nano Materials, 2021, 4 (12), pp.14035-14046. 10.1021/ac-sanm.1c03322 . hal-03725169

**HAL Id: hal-03725169**

**<https://hal.science/hal-03725169>**

Submitted on 15 Jul 2022

**HAL** is a multi-disciplinary open access archive for the deposit and dissemination of scientific research documents, whether they are published or not. The documents may come from teaching and research institutions in France or abroad, or from public or private research centers.

L'archive ouverte pluridisciplinaire **HAL**, est destinée au dépôt et à la diffusion de documents scientifiques de niveau recherche, publiés ou non, émanant des établissements d'enseignement et de recherche français ou étrangers, des laboratoires publics ou privés.

# Controlled Nanoconfinement of Polyimide Networks in Mesoporous $\gamma$ -Alumina Membranes for Molecular Separation of Organic Dyes

*Nikos Kyriakou,<sup>a</sup> Louis Winnubst,<sup>a,\*</sup> Martin Drobek,<sup>b</sup> Sissi de Beer,<sup>c</sup> Arian Nijmeijer,<sup>a</sup> and Marie-Alix Pizzoccaro-Zilamy<sup>a,\*</sup>*

<sup>a</sup> Inorganic Membranes, MESA+ Institute for Nanotechnology, University of Twente, 7500 AE Enschede, The Netherlands

<sup>b</sup> Institut Européen des Membranes, UMR5635, CNRS-UM-ENSCM, Université de Montpellier (CC047), Place Eugène Bataillon, 34095 Montpellier Cedex 5, France

<sup>c</sup> Sustainable Polymer Chemistry Group, Department of Molecules & Materials, MESA+ Institute for Nanotechnology, University of Twente, 7500 AE Enschede, The Netherlands

**KEYWORDS:** Polyimide, nanoconfinement, mesoporous  $\gamma$ -alumina membranes, solvent resistant nanofiltration, organically modified membranes, surface-induced *in-situ* polymerization.

**ABSTRACT:** Polyimide networks are key in the development of stable, resilient, and efficient membranes for separation applications under demanding conditions. To this aim, the controlled design of the network's nanostructure and its properties are needed. Yet, such control remains a challenge with the currently available synthesis methods. Herein, we present a simple nanofabrication approach that allows the controlled nanoconfinement, growth and covalent attachment of polyimide (PI) networks inside the mesopores of  $\gamma$ -alumina layers. The attachment of the PI network on the  $\gamma$ -alumina layer was initiated via

different pre-functionalization steps who play a pivotal role in inducing the *in-situ* polymerization reaction at the pore entrance and/or at the inner pore surface. The nanoconfinement was found to be limited to maximal the 1.5  $\mu\text{m}$  thick  $\gamma$ -alumina supporting layer and the resulting hybrid PI/ceramic membranes showed stable performance in a variety of solvents. These PI/ceramic membranes were found to be very efficient in the challenging separation of small organic dye molecules such as Rhodamine B ( $479 \text{ g mol}^{-1}$ ) from toxic solvents such as dimethylformamide or dioxane. Therefore, this technique opens up possibilities for a multitude of separations. Moreover, the PI synthesis approach can be applied to other applications that rely on porosity and stability control as well, such as for advanced insulation and anticorrosion.

## INTRODUCTION

Industry relies heavily on separation methods, from the purification of primary materials to the isolation of polymers, pharmaceuticals, and many other products.<sup>1</sup> Conventional separation methods, such as distillation, are principally thermally driven. As a result, they can be costly, energy intensive and inefficient in separating thermally sensitive intermediates or products.<sup>1-3</sup> As an alternative, nanofiltration membrane-based separation technologies are increasingly implemented in industry in either combination with distillation or extraction as hybrid processes or by totally replacing these conventional methods. The term “nanofiltration” (NF) refers to a pressure-driven membrane-based separation process in which particles and dissolved molecules smaller than 2 nm are rejected. By replacing the high energy-demanding thermally-driven separation methods (e.g. distillation) with low energy-demanding pressure-driven NF membranes, one can get more energy-efficient and environmentally-friendly processes.<sup>1-3</sup> Nevertheless, current membrane materials, which are often polymeric, are not always compatible with industrial streams, particularly mixtures of water and organic solvents, causing membrane failure due to degradation or dissolution of the

material itself. Therefore, when designing a membrane for complex applications, one should consider not only the mixture of solutes but also the nature of the solvents involved.

Nowadays, membranes developed for such challenging applications are called solvent-tolerant nanofiltration membranes (STNF).<sup>2,4</sup>

The most common materials used to prepare STNF membranes are polymers, like polyamide-imides,<sup>5</sup> polydimethylsiloxanes,<sup>6</sup> etc. These polymeric membranes have generally shown high permeability and stable rejection with polar organic solvents such as alcohols or tetrahydrofuran. Yet, the performance of these membranes is unsatisfactory in presence of apolar solvents, mainly due to the degradation of the supporting layer.<sup>4</sup> As a result, the permeability often becomes lower and the rejection unpredictable. Hence, such behavior hinders the implementation of this membrane technology in water/solvent streams. The combination of a chemical-inert porous ceramic support, functionalized with polyimides (PI), can overcome the instability issue of the support. PI are among the most resilient polymeric membrane-based materials used nowadays. PI are polymers characterized by a stable imide ring as a repetitive unit that exhibits good mechanical properties, chemical solvent resistance, heat resistance, and electrical properties.<sup>7</sup>

Polyimides are prepared by the polycondensation reaction between (di)anhydrides and (di or tri) amines at temperatures between 180 and 300 °C. Due to their high thermal (> 400 °C) and chemical resistance, polyimides are extensively used as membrane materials for applications in gas separation, solvent exchange, and many others.<sup>8</sup> Commercial PI membranes such as Puramem® were found well adapted for specific STNF applications in solvents such as toluene and heptane, but only in operating conditions up to 50°C.<sup>9</sup> To prevent dissolution and to increase the hydrophilicity (imide group to amic acid) of the PI membrane material in polar aprotic or chlorinated solvents, it has been reported that additional cross-linking steps are often needed.<sup>8</sup> Even though, the amic acid is more hydrophilic than imides,

they nevertheless are less chemically stable.<sup>10</sup> Therefore, in membrane technology it is crucial to combine a high stable material, such as polyimides, which are also potentially processable to membranes. Therefore different approaches were explored to overcome the problems associated with material stability and processability.<sup>11</sup> For example, Kuttiani Ali et al.<sup>12</sup> developed hydrophilic nanocomposite membranes for ultrafiltration by adding silica nanoparticles, pre-functionalized with deep-eutectic solvents, into a polyimide solution prior to casting. The membranes containing 2 wt.% of nanoparticles presented the best mechanical and phenol retention under a wide pH range. Moreover, recently, Wei et al.<sup>13</sup> prepared an ultrathin polyimide/silica nanofiltration membrane by *in-situ* hydrolysis and condensation of tetraethoxysilane. The resulting membrane presented improved hydrophilicity, mechanical strength, and thermal stability compared to the pure PI-NF membrane. By using a similar approach, Qiang et al.,<sup>14</sup> formed a resistant STNF membrane. Despite the promising performances, the potential leaching of nanoparticles is not negligible and can lead to potential human and environmental exposure.<sup>15</sup> Thus far, many researchers have focused on introducing inorganic nanoparticles into the PI matrix. The opposite approach in which PI networks are confined in an inorganic matrix could also be employed.

Following this latter strategy, Isaacson et al.<sup>16,17</sup> nanoconfined a PI network in a mesoporous tortuous organosilica matrix. The preparation procedure involved infiltrating polyamic acid oligomers into the porous matrix and subsequent cross-linking of the polymer units. As a result, the composite film/layer prepared showed enhanced resistance to fracture compared to the pristine mesoporous support, due to a so-called confinement-induced molecular bridging mechanism. Such confined polyimide systems could be used as a thermal barrier coating for high-temperature operations (at least up to 350 °C) and superior lightweight materials for aerospace applications. However, the possibility to use this confined PI network as a separation layer is unknown.

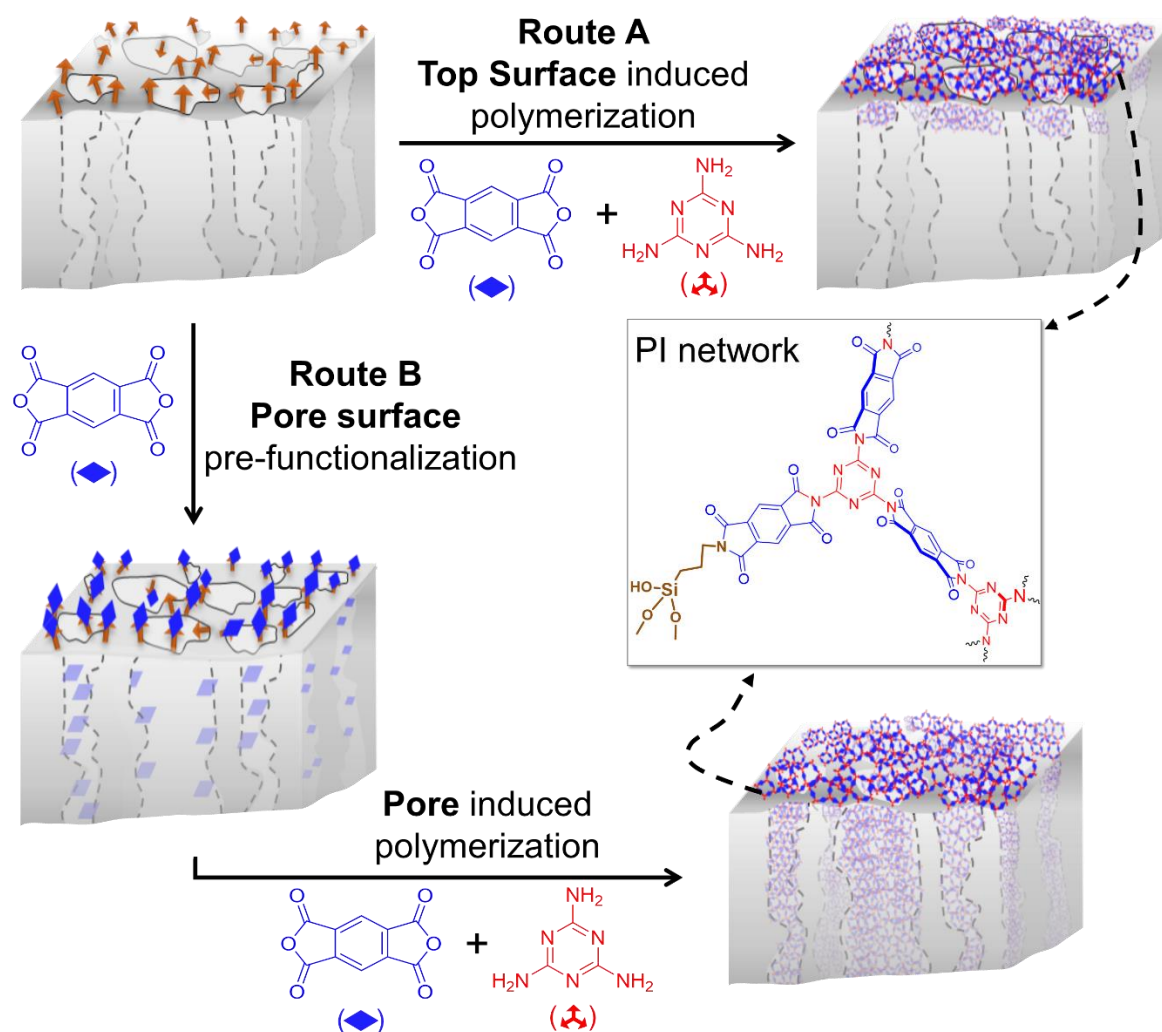
Studies have shown that the nanoconfinement of a crystallized polymer within nanoporous anodic aluminum oxide (AAO) templates is a suitable approach to prepare innovative systems for biosensing, optical and electrical-related applications.<sup>18</sup> When a polymer is confined within a micrometer thick rigid AAO template, comprising of vertically oriented large pores (10-100 nm) which are not tortuous, the crystallization behavior experiences dramatic changes as the pore size is reduced. This approach allows to modulate the polymer nanostructures for specific applications but is not suitable for practical separation applications in industry due to the limited surface area of the AAO supports when dealing with cubic meter of water and their fragility when exposed to harsh conditions.<sup>19</sup> In contrast to previous studies done on AAO support or mesoporous organosilica layer, we looked at defined and rigid mesoporous ceramic membranes with relatively low tortuosity. Alumina ( $\gamma$ , or  $\alpha$  phase) membranes are commercially predominant in the market and are available in the shape of discs and tubes.<sup>20,21</sup> Compared to AAO templates, mesoporous  $\gamma$ -Al<sub>2</sub>O<sub>3</sub> membranes are supported on millimeter thick  $\alpha$ -alumina supports, and commercialized in the form of modules, making them suitable for real separations under demanding conditions (high pressure and temperature).<sup>22,23</sup> However, due to their relatively large pores (~5 nm), they are not selective in the nanofiltration range. Nevertheless, the  $\gamma$ -alumina surface is rich in free hydroxyl groups that can be used to modify the pore entrance and inner pore surface by covalently attaching molecules, oligomers, and polymer brushes to prepare hybrid membranes.<sup>4,24–27</sup>

In fact, it has been shown that grafting-to and grafting-from reactions can be applied to modify dense substrates<sup>28</sup> but also the pore entrance and inner pore surface of  $\gamma$ -alumina mesoporous layers.<sup>4,24–27</sup> Sun et al.<sup>28</sup> used the grafting-from method to grow polyglycidyl methacrylate brushes from the surface (-induced) of silicon wafers. These brushes were utilized as an adhesive interlayer for chemically attaching a polyimide film on silicon wafers. As a result, improved friction and wear resistance was observed, compared to the polyimide

films on bare silicon wafers. However, the possibility of simultaneous pore confinement and covalent attachment of a crosslinked PI network onto the ceramic support has not been demonstrated yet. Furthermore, the growth of a crystalline polymer in one step from the surface of a ceramic support as well as the applicability of such material under membrane conditions is still not shown in literature.


In this work, we have initiated for the first time the *in-situ* polymerization reaction of a PI network directly from an inorganic surface, and controlled the nanoconfinement inside rigid and well-defined, tortuous  $\gamma$ -alumina mesoporous  $\gamma$ -alumina mesoporous layers as indicated in Scheme 1. Our strategy is to use two different precursors that promote the confinement of the PI network in the ceramic support. The first precursor, bearing an amino-functional group, is located at the top surface and pore entrance, while the second one, consisting of an anhydride-functional group, is present on both the surface and within the mesopores of the  $\gamma$ -alumina layer. Indeed, the above functional groups induce a surface polyimidization reaction that controls the location of the network formation either at the pore entrance or inside the  $\gamma$ -alumina layer. Furthermore, we show that by increasing the reaction time from 1 to 5 days, the membrane performance was significantly improved due to increase in concentration of the polyimide network into/on the mesoporous layer. To demonstrate the successful growth and confinement of the polymer inside the mesoporous layer, a combination of different surface and pore characterization techniques were employed. In addition, the nanoconfined PI-based membranes were tested in different model mixtures where its potential as solvent-resistant nanofiltration (NF) membrane was demonstrated. The concept described in this work, illustrates how a cross-linked polyimide can grow in a nanoconfined space, such as the tortuous but defined mesopores of our alumina membranes. This can be achieved by simply controlling the grafting of the initiator for the surface-induced in-situ polymerization from the surface of the alumina support.

This approach can be expanded in other fields where controlled nanoconfinement of a crosslinked crystalline polymer is desired for different applications.



**Scheme 1.** Schematic illustration of the two fabrication routes, A and B, used for the controlled nanoconfinement of the PI network in a tortuous but defined, rigid mesoporous  $\gamma$ -alumina layer matrix. Both routes originate from pre-functionalized supports with APTES molecules ( $\leftarrow$ ) grafted at the top surface of the support. In route A, a direct growth of the PI takes place, between PMDA ( $\blacklozenge$ ), MA ( $\blacktriangle$ ) and the superficial amino-functionality, leading to the formation of the PI network at the top surface and pores entrance. In route B, an additional pre-functionalization of the APTES-modified support (top and pore surface) is



conducted with dianhydride (PMDA, ) molecules. Via this route, the subsequent PI network formation is also extended (favored) inside the  $\gamma$ -alumina mesopores.

## RESULT AND DISCUSSION

**Synthesis and characterization of the pre-functionalized  $\gamma$ -alumina layer and polyimide membranes.** Our strategy to pre-functionalize supports and subsequently form the polyimide (PI)-based membranes is presented in Scheme 1. The PI nanoconfined membranes were prepared by the pre-functionalization of the mesoporous  $\gamma$ -alumina layer with 3-aminopropyl trimethoxysilane (APTES). A reliable vapor phase grafting procedure has been developed by our research group to covalently attach APTES molecules at the pore surface of the  $\gamma$ -alumina layer. Indeed, carefully selecting the grafting conditions and a suitable pore filling agent can lead to a homogeneous monolayer of APTES molecules without the problem of homocondensation reactions occurring between the alkoxy silane linking group.<sup>24</sup> The primary amine group of APTES can react *via* a condensation reaction with the dianhydride precursor of the PI network during the subsequent polyimidization reaction between pyromellitic dianhydride (PMDA) and melamine (MA). This reaction should lead to the covalent attachment of the polyimide network exclusively on the top surface and pore entrance of the mesopores  $\gamma$ -alumina- layer (Scheme 1, route A). Here, we employed a pore blocking agent allowing us to graft only the top surface and pore entrance of the  $\gamma$ -alumina layer. Hence, we assume that the rapid PI network formation from the functionalized pore entrance will limit the diffusion of monomers as well as any PI oligomer units formed in the bulk solution into the pristine pores. In this way, a PI concentration gradient is induced along the mesoporous layer with the highest concentration close to the pore entrance. To allow for the PI network formation to occur also inside the mesopores of the support, samples were modified in solution with only PMDA before the *in-situ* polycondensation (Scheme 1, route B). Here, PMDA can react not only with the amino group of the grafted APTES molecules

but also with free hydroxyl groups at the inner pore surface of  $\gamma$ -alumina layer.<sup>29</sup> Thus, the PI network formation takes place uniformly from the whole surface, including pore entrance and pore surface, of the mesoporous  $\gamma$ -alumina layer.

Fourier transform infrared (FTIR) analysis was employed to demonstrate the pre-functionalization of the mesoporous  $\gamma$ -alumina layer. The spectra of the pristine  $\gamma$ -alumina layer and the layers pre-functionalized respectively with APTES (sample A) and APTES+PMDA (sample B) are shown in Figure 1a. The FTIR spectrum of the pristine mesoporous layer shows a broad band centered at  $3420\text{ cm}^{-1}$  which can be attributed to the stretching vibration of adsorbed water and surface hydroxyl groups.<sup>30,31</sup> Functionalization of the  $\gamma$ -alumina layer with APTES results in the appearance of primarily a broad band between  $1180$  and  $970\text{ cm}^{-1}$  which is associated with the formation of the Al-O-Si bond and confirms the grafting of the APTES at the top surface and pore entrance. This finding is further confirmed by the presence of the asymmetric and symmetric stretching vibration bands at  $2927$  and  $2886\text{ cm}^{-1}$  which can be attributed to the alkyl groups ( $-\text{CH}_2-$ ) of the grafted APTES molecules. In addition, the sharp vibration band at  $2974\text{ cm}^{-1}$  (Figure S4) attributed to the linking function ( $\text{CH}_3\text{-CH}_2\text{OSi}$ ) is not present in the spectrum of sample A, suggesting complete hydrolysis of the functional group during the grafting reaction and thus confirms the formation of the desired Si-O-Al bond again.<sup>24</sup> In comparison with sample A, the interpretation of the FTIR spectrum of sample B is more difficult due to the number of absorption bands detected. Instead of attributing each vibration band, only the most important ones are discussed here. The formation of the imide functional group and attachment of PMDA is confirmed first by the vibration bands at  $1787$  and  $1727\text{ cm}^{-1}$ , ascribed to the C=O bond, and the band at  $1365\text{ cm}^{-1}$ , related to C-N-C bond. In addition, the anhydride group is also apparent at  $1856\text{ cm}^{-1}$  which suggests either the partial reaction of PMDA with the amino-functionalized support (A) and/or the presence of unreacted and physically adsorbed

PMDA on the ceramic support. The band at  $2460\text{ cm}^{-1}$  attributed to the carboxylate groups ( $\text{COO}^-$ )<sup>32</sup> in the sample is due to the formation of amic acid group or due to PMDA grafting at the pore surface.<sup>29,32</sup>

Cyclohexane permoporometry was used to study the effect of pre-functionalization on the pore size distribution of the support. This dynamic characterization technique allows measuring the pore diameter of active pores present in the pre-functionalized  $\gamma$ -alumina layer. The stepwise analysis will enable one to follow the change in pore diameter starting from the pristine  $\gamma$ -alumina layer and moving towards the functionalized samples (A and B in Figure 1b). The pristine  $\gamma$ -alumina layer exhibits a mean pore diameter of  $\sim 5.5\text{ nm}$  and the support pre-functionalized with APTES (sample A) shows no pore size diminution. This last result differs from published reports where a pore shrinkage of  $0.5\text{ nm}$  was observed, where no glycerol or other pore-blocking agents were used.<sup>33</sup> This means that glycerol, used as the pore blocking agent, has allowed us to control the grafting reaction and to functionalize only the top surface of the  $\gamma$ -alumina layer. However, subsequent functionalization with PMDA (sample B) resulted in a significant reduction of the pore diameter. Compared to pristine  $\gamma$ -alumina and sample A, the oxygen permeation curve of sample B presented in Figure 1b suggests that the pore opening occurs at low cyclohexane relative pressures during the desorption step ( $\approx 0.1$  instead of  $0.4\text{ P/P}_0$ ). Considering the data acquired *via* cyclohexane permoporometry, we cannot determine the exact pore diameter since the Kelvin equation is not valid due to the very unclear transition point obtained for this sample. Nevertheless, knowing the limit of the measurement, which corresponds to the molecular diameter of cyclohexane ( $\sim 0.5\text{ nm}$ ), one can assume that the pore diameter of the sample B must be lower than  $1\text{ nm}$ . Overall, the cyclohexane permoporometry results indicate the presence of PMDA in the pores of the  $\gamma$ -alumina layer, which can be physically or chemically adsorbed at the pore entrance and inner pore surface.

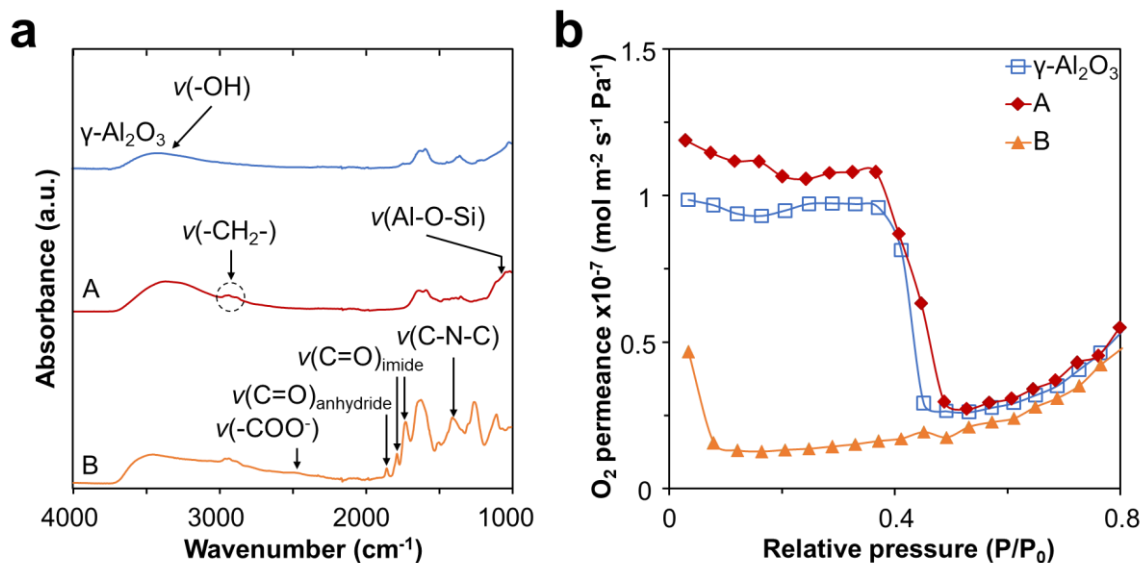


**Figure 1:** (a) FTIR spectra of the pre-functionalized samples (A (red) and B (orange)) and comparison with the pristine  $\gamma$ -alumina layer ( $\gamma\text{-Al}_2\text{O}_3$ ) in the interval between 1000 and 4000  $\text{cm}^{-1}$ . (b) Oxygen permeance as function of the relative cyclohexane vapor pressure for the pristine  $\gamma$ -alumina layer, sample A and B. The oxygen flux is measured only through active pores in the range of 2 – 50 nm. Using the Kelvin equation, the pore diameter distribution can be estimated for the pristine  $\gamma$ -alumina layer and the sample A as shown in Figure S19. However, the pore diameter of B is below the molecular size of cyclohexane (condensable liquid). Thus, pore size distribution cannot be estimated in this way.

As explained before, the attachment, growth and molecular confinement of the PI network in the  $\gamma$ -alumina layer was performed *via* two different approaches; firstly, by the direct formation of the PI network from the pre-functionalized surface of sample A, where the functional groups were at the top surface and pore entrance of the  $\gamma$ -alumina layer and secondly, from sample B, where the functional groups were located at the top and pore surface of the  $\gamma$ -alumina layer. FTIR analysis was performed on the nanoconfined PI membranes to assess the spectroscopic characteristics of the network formed after *in-situ* polymerization. Figure 2a displays the spectra of the four PI nanoconfined membrane samples

(A-1/5 and B-1/5). All samples exhibit similar spectroscopic characteristics with minor differences in the intensity of certain bands for the two different reaction times (1 and 5 days) and both reaction routes. The two bands at  $\sim 1780$  and  $\sim 1720\text{ cm}^{-1}$  are ascribed to the C=O bond of the imide and are more intense with longer reaction times for both routes. The bands at  $1565$  and  $1453\text{ cm}^{-1}$  are attributed to the stretching vibration of the triazine ring and appear in all membranes.<sup>34</sup> The band at  $1660\text{ cm}^{-1}$  could indicate the presence of amic acid on the  $\gamma$ -alumina layer. However, no other absorption bands confirm the presence of amide. To get a better insight into this observation, the powders (I-1 and I-5) collected from the reaction mixture were used to indirectly gain information on the nature of the material, confined in the mesopores (Figure S13 and S14). The FTIR spectra of the powders, formed in the bulk solution during *in-situ* polymerization of membrane samples, clearly show the formation of an amino-terminated imide network. Hence, *in-situ* polymerization seems to promote imide formation for both 1- and 5-days reaction time, without any indications of amic acid presence. Finally, the band between  $1390$  and  $1360\text{ cm}^{-1}$  is ascribed to the absorption of the C-N-C group.<sup>35–37</sup> Thus, leading to the conclusion that the FTIR analysis strongly suggests the presence of a polyimide network in the  $\gamma$ -alumina layer.

The high crystallinity of aromatic polyimides has been demonstrated in the literature by powder X-ray diffraction (XRD) analysis.<sup>7</sup> In our work, no diffraction peaks corresponding to crystalline aromatic polyimides could be detected in the membrane samples (Figure S15). The XRD pattern obtained revealed the presence of the highly intense diffraction peaks of the  $\alpha$ -alumina macroporous support which can be explained by X-rays' penetration depth (being more than  $3\text{ }\mu\text{m}$  in the XRD configuration used). The absence of diffraction peaks correlated with the  $\gamma$ -alumina phase where the polyimide network is confined can be explained by the nanosized nature of this layer. Kim et al.<sup>38</sup> described a decrease in the diffraction peaks of the  $\alpha$ -alumina phase when different polyimide/ $\alpha$ -alumina film composites were prepared using an

amorphous polymer. Interestingly, the diffraction peaks of the  $\alpha$ -alumina phase were identical with our pristine support, thus suggesting either small amounts or even absence of the PI network in the  $\alpha$ -alumina pores. To shed more light into the confined network's nature, XRD analysis was conducted on the powder extracted from the bulk solution at the end of the synthesis of the membranes. The powder XRD patterns between  $5 - 50^\circ 2\theta$  are provided in Figure S16 for the powder samples obtained after 1 or 5 days of reaction times (denoted as I-1 and I-5). The analysis revealed the formation of polycrystalline materials with an amorphous background observed in small proportion. Comparison of the diffractograms between samples I-1 and I-5 show a clear relationship between increasing reaction time and improved crystallinity, evidenced by the narrowing of the diffraction peaks and a decrease in the baseline broadening. These results are corroborated by the scanning electron microscopy (SEM) analysis of the powders (Figure S20) which also show changes in morphology as a function of reaction time. The sample I-1 appeared to consist of a mixture of platelet crystallites of several micrometer wide, cauliflower-like aggregates and clustered (random) spherical porous phases (ranging from nanometers to micrometers in diameter). Increasing reaction time led to the growth of a fascinating morphology consisting of defined flower-shaped crystallites, as observed with sample I-5, decorated with smaller crystallites. Similar results were obtained by Baumgartner et al.<sup>7,39</sup> who observed an "amorphous" baseline while analyzing the produced polyimide crystalline samples under hydrothermal conditions, using p-phenyldiamine and PMDA as monomers. Comparison with published records of polyimide powders prepared using the same precursors (PMDA and MA) but under different experimental conditions (temperature and solvent) shows different crystal structures. Li et al.<sup>35</sup> described the preparation of a PI powder between PMDA and MA below  $200^\circ\text{C}$  leading to a relatively amorphous material (two broad peaks between  $10$  and  $50^\circ$ ), whereas at  $200^\circ\text{C}$  or above<sup>40</sup> a semi-crystalline structure was observed. Thus, the powder XRD results provided

here confirm that the organization of the material depends both on the temperature of the polycondensation reaction and the reaction times. However, when the PI powder was treated at 300 °C for several hours, a new diffraction peak at 44° was observed, which is possibly related to degradation by-products. Thermal treatment of the PI powders at 400 °C, resulted in almost complete loss of crystallinity and increase in intensity of the diffraction peak at 44° (Figure S17). The observed thermal degradation evidenced by powder XRD, is also corroborated by the thermogravimetric analysis (TGA) provided in Figure S18. A small weight loss for both I-1 and I-5, 2.2% and 1.4%, respectively, occurred upon heating from room temperature to 300°C. However, above 300 °C a significant weight loss occurs, particularly for sample I-1. Thus, we can assume that the PI network remains stable at temperatures below 300 °C, which is ideal for membrane applications.

It must be noted that the confinement of a polyimide network in the  $\gamma$ -alumina layer should lead to an enhancement of the physicochemical stability of the polyimide network as shown by Isaacson et al.<sup>17</sup> Based on the powders' crystallinity and morphology, one can assume that the PI membrane samples exhibit similar structural characteristics as the polyimide powders. If our assumptions are confirmed, it would mean that by simply varying the reaction time, we can engineer the membrane's micropores and thus enhance the membrane separation performance. Therefore, it is crucial to look closer at the PI network inside the support and well describe the nanoconfinement effect.

**PI network nanoconfinement characteristics.** A series of analytical techniques were employed to investigate the influence of the supports' pre-functionalization on the extend of the PI nanoconfinement. First, water contact angle analysis was done on the PI nanoconfined samples and the pristine support to evaluate (indirectly) the polymerization effect on the support surface properties. The results are given in Figure 2b. Compared to the pristine layer, which presents a water contact angle of 14° (disappears in 6 – 7 seconds) characterizing

porous hydrophilic surface, the PI nanoconfined samples show an increased water contact angle ( $40 - 65^\circ$ ). This observation suggests that the membrane surface is still hydrophilic (water contact angles  $< 90^\circ$ ) but certainly less than the pristine support. Interestingly, different water contact angles were obtained for the samples prepared *via* route A and B, respectively  $63^\circ (\pm 16^\circ)$  and  $54^\circ (\pm 5^\circ)$  for the same reaction time (1 day). Nevertheless, with the increase of the reaction time, a rise of  $11^\circ$  was measured for the samples prepared *via* route B, while a decrease of  $19^\circ$  was measured for the samples made *via* route A. As for porous hydrophilic surfaces, accurate estimation of a descending water contact angle is challenging. Still, the difference observed between the two routes can be inherent to the pre-functionalization step.

Further investigation and comparison of the PI-nanoconfined membrane surface morphology with that of the  $\gamma$ -alumina layer was conducted by atomic force microscopy (AFM) analysis, and the results are shown in Figure 2c. From the average roughness profiles, it is apparent that the surface morphology of the PI nanoconfined membranes changes with increasing reaction time. Compared with the pristine  $\gamma$ -alumina layer, polymerization for 1-day, for both routes, does not seem to affect the surface roughness ( $\sim 3$  nm). Samples reacted for 5 days, show only slight increase in surface roughness ( $\sim 4$  nm) with the A-5 samples exhibiting larger differences in height on the surface than for B-5 ( $\sim 3$  nm) as shown in Figure 2c. The empirical information gained from water contact angle and AFM analyses postulate a fundamental difference between the two routes, which becomes more prevalent after longer reaction times. The influence of reaction conditions on the pore diameter of the PI nanoconfined membranes was investigated by means of cyclohexane permoporometry. The results are provided in Figure 2d. During the analysis, no oxygen permeation was measured at low cyclohexane partial pressures ( $< 0.55$ ), which indicates the presence of micropores (pore diameter  $< 1.5$  nm) or even of a dense sample. This suggests a pore diameter shrinkage of



more than 4 nm. Indeed, the permporometry analysis demonstrates that the presence of the PI network affects the pore size of the mesoporous  $\gamma$ -alumina layer.

All the results described above showed that the polymer network changes the morphology of the surface only in a subtle manner. However, the pore sizes are significantly affected, indicating either an ultrathin top layer or a confined polymer in the mesoporous layer. To better understand this finding and to observe the PI network on the  $\gamma$ -alumina layer directly, we proceeded with HR-SEM analyses of the studied membrane samples.

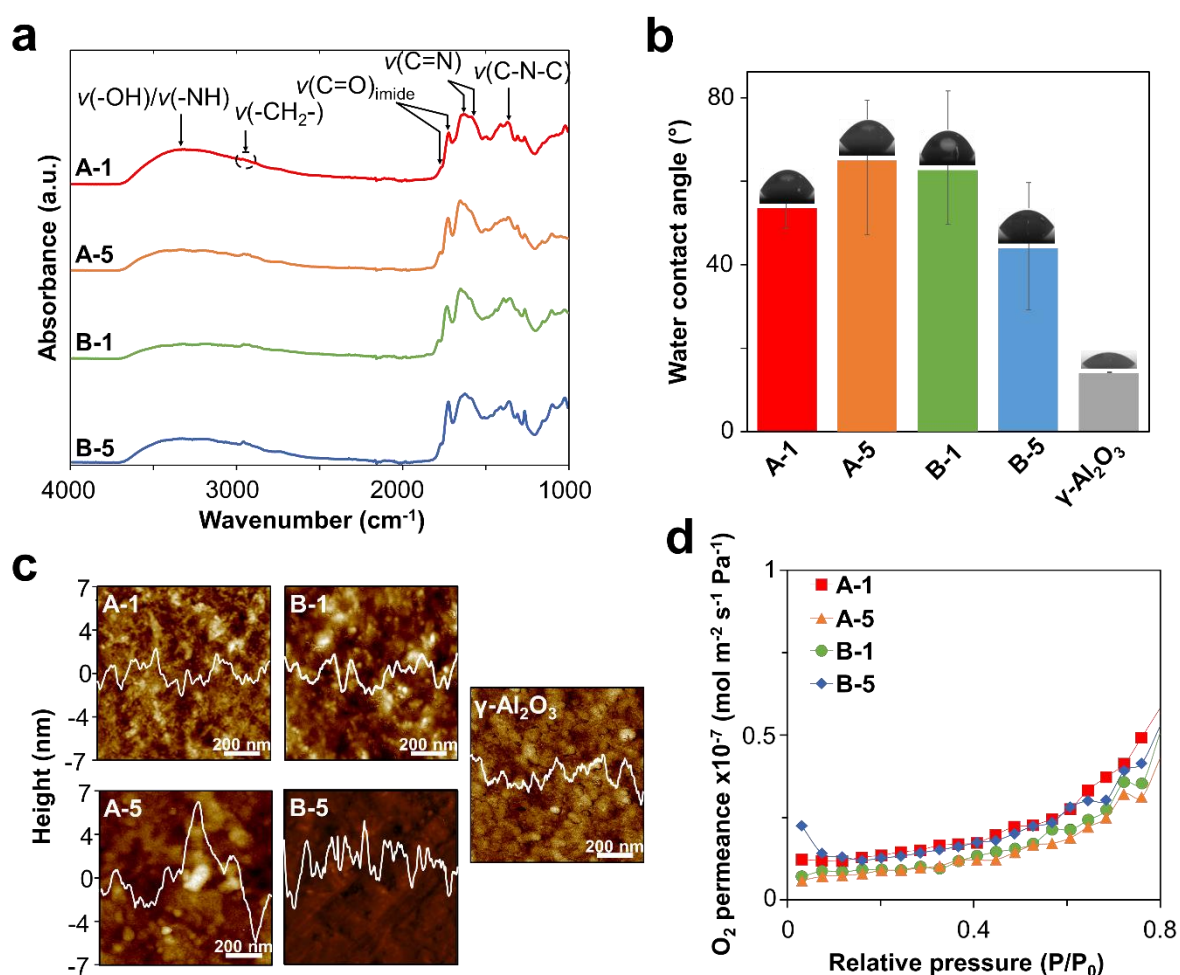


**Figure 2:** (a) FTIR analysis of the PI nanoconfined samples. The complete spectra between 4000 and 400  $\text{cm}^{-1}$  are provided in SI. (b) The water contact angle of the PI nanoconfined samples. (c) AFM micrographs of the top surface of the PI nanoconfined samples and the

pristine  $\gamma$ -alumina layer. The line represents the averaged roughness profile of each sample.

(d) Oxygen permeation as a function of cyclohexane partial pressure of PI nanoconfined membranes.

The top surface and cross-section High-Resolution SEM pictures of the PI nanoconfined membranes are given in Figure 3a, together with photographs of the membrane samples. Compared to the pristine  $\gamma$ -alumina layer, which is naturally white (Figure S21), the PI nanoconfined membrane samples appear to be substantially covered by the polymeric network as denoted by the brownish coloration, typical for a polyimide material. Comparison of the top-surface micrographs of membrane samples prepared by the two fabrication routes (A and B) does not show any significant differences at first glance. One day of reaction leads to the formation of small particles with a sheet-like structure visible on both A-1 and B-1 samples. Increasing the reaction time to 5 days leads to the disappearance of the sheet structure, suggesting the formation of a thin homogeneous layer. From the SEM analysis of PI powders (Figure S20) we observed that the 5-day long reaction yields a clear platelet-like structure, whereas the 1-day reaction results in a mixture of aggregates and crystallites. From the HR-SEM analysis of the top surface of both A-1 and B-1 samples, one can observe similar sheet-like structures. This indicates that the PI networks that are growing on the surface of the  $\gamma$ -alumina layer and those growing in the bulk solution exhibit similar characteristics. Hence, we expect that the PI network growth, induced from the ceramic surface, will have a similar morphology with smaller particles, mainly when infiltrated in the pores. Finally, it is expected that such platelet-like particles should ensure good coverage of the support surface, as seen on the micrographs of both A-5 and B-5 samples.

In comparison, the HR-SEM cross-sectional analysis of the membranes show a clear difference between the two synthesis routes after 1 day of reaction. For the A-1 sample, the PI network seems to be located at the  $\gamma$ -alumina layer top surface. In contrast, for the B-1

sample, infiltration of the PI network in the  $\gamma$ -alumina layer could be observed. The samples after 5 days of reaction time, respectively A-5 and B-5, also present extended infiltration of the PI network in the  $\gamma$ -alumina layer. This finding thus strongly indicates that longer reaction times of polymerization on pre-functionalized  $\gamma$ -alumina layers promoted the nanoconfinement of the PI network in the 5 nm pores of the  $\gamma$ -alumina layer. Evidently, the difference between the membranes A-1 and B-1 suggests that the choice of pre-functionalization can affect the extent of the PI nanoconfinement in the  $\gamma$ -alumina layer.

In complement, energy-dispersive X-ray spectroscopy (EDS) analysis can offer qualitative elemental information over a membrane's cross-section (Figure 3b). By measuring the ratio of carbon over aluminum along the cross-section of the different membrane samples, one can define the influence of the preparation route, and indirectly the pre-functionalization steps on the nanoconfinement of the PI network. Overall, the EDS analysis reveals that organic (polymeric) material resides in the  $\gamma$ -alumina layer. In route A, the network accumulates near the pore entrance, whereas in route B (samples B-1 and B-5), a spread distribution of the PI network inside the  $\gamma$ -alumina layer was observed. These results thus clearly indicate a link between the pre-functionalization step and the nanoconfinement of PI network inside the  $\gamma$ -alumina layer. On the hand, the reaction time merely affects the concentration of the polymeric network.

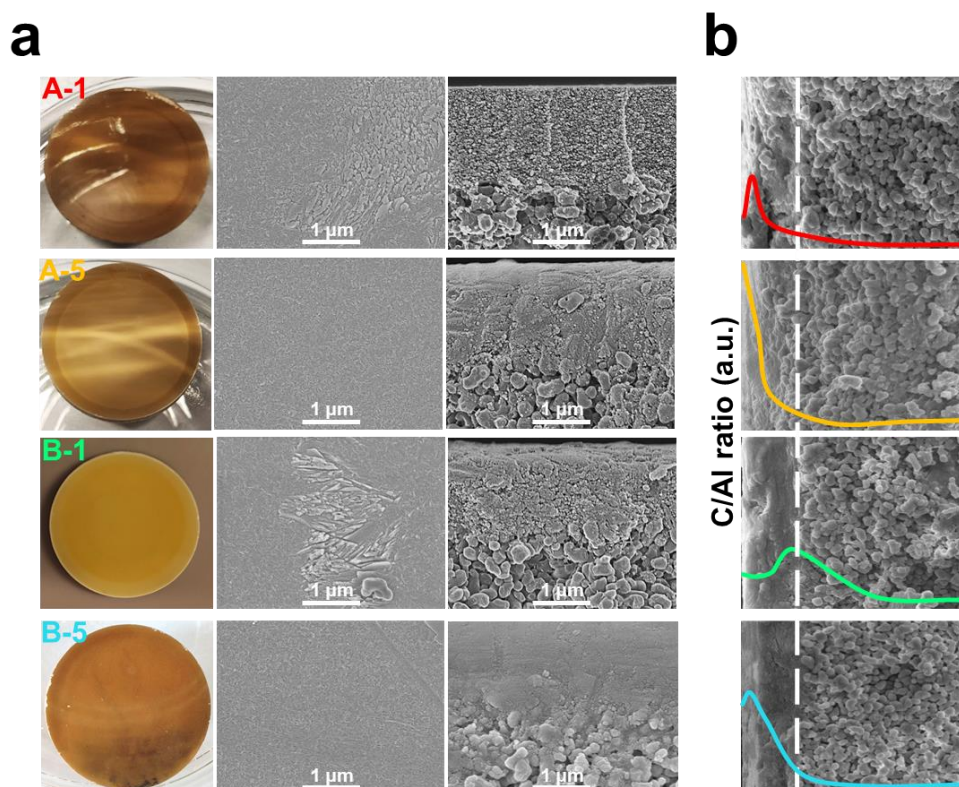


**Figure 3:** (a) Images of the PI nanoconfined membranes (left) accompanied with HR-SEM micrographs of top surfaces (middle) and the cross-sections (right). (b) Evolution of carbon/aluminum ratio (wt.% by EDS) along the membrane cross-section. The broken white line denotes the limit between the  $\gamma$ -alumina layer (left) and the  $\alpha$ -alumina support (right).

In conclusion, by combining the knowledge gained from HR-SEM and EDS, we can assure that the functionalization of the support promotes the growth of the PI network during polymerization. Based on these results, a membrane formation mechanism was drawn (Scheme 1). The membranes prepared *via* route A, thanks to the presence of the amino group (APTES) at the top surface of the support, exhibit a higher concentration of PI near the pore entrance. Alternatively, with route B, a homogeneous polymer distribution is observed throughout the  $\gamma$ -alumina layer, which is attributed to the functionalization of the inner pore surface with anhydride functional groups (PMDA). These differences in membrane architecture can significantly affect their membrane performance due to an increase in the

thickness of the separating layer, as schematically shown in Scheme 1. Additionally, longer reaction times lead to higher concentrations of polymer inside the  $\gamma$ -alumina layer, which could potentially promote formation of smaller pore diameters, and thus better separation performance. To confirm our interpretation from the HR-SEM and EDS analysis, a series of membrane separation tests have been performed with model water solutions described hereafter.

**PI nanoconfined membranes performance.** The PI nanoconfined membranes were tested first in aqueous solutions of Brilliant Yellow (BY,  $625 \text{ g mol}^{-1}$ ) or Rhodamine B (RB,  $479 \text{ g mol}^{-1}$ ) and compared with the pristine  $\gamma$ -alumina layer. The retention and water permeability results are summarized in Figure 4. All four PI nanoconfined membranes show retentions above 90% of BY ( $627 \text{ g mol}^{-1}$ ) in water, which is a significant increase compared to the pristine  $\gamma$ -alumina layer (76%). However, with Rhodamine B (RB,  $479 \text{ g mol}^{-1}$ ), the retentions for the A-1 and B-1 samples were between 70-80%. With increasing the polyimidization reaction time, the membranes (A-5 and B-5) show RB retentions well over 90%. This can be attributed to increasing PI concentration in the pores of the  $\gamma$ -alumina layer. Compared with the pristine  $\gamma$ -alumina layer (14% retention for RB), the separation performance of the PI nanoconfined membranes thus displays a significant improvement. These results also suggest that, despite this increase in concentration of the polymeric network in the tortuous mesopores, there are still many open pores that are either smaller than the Rhodamine B molecule (sieving effect) or are small and charged (Donnan effect) and thus have a direct influence on the separation performance of the membranes.

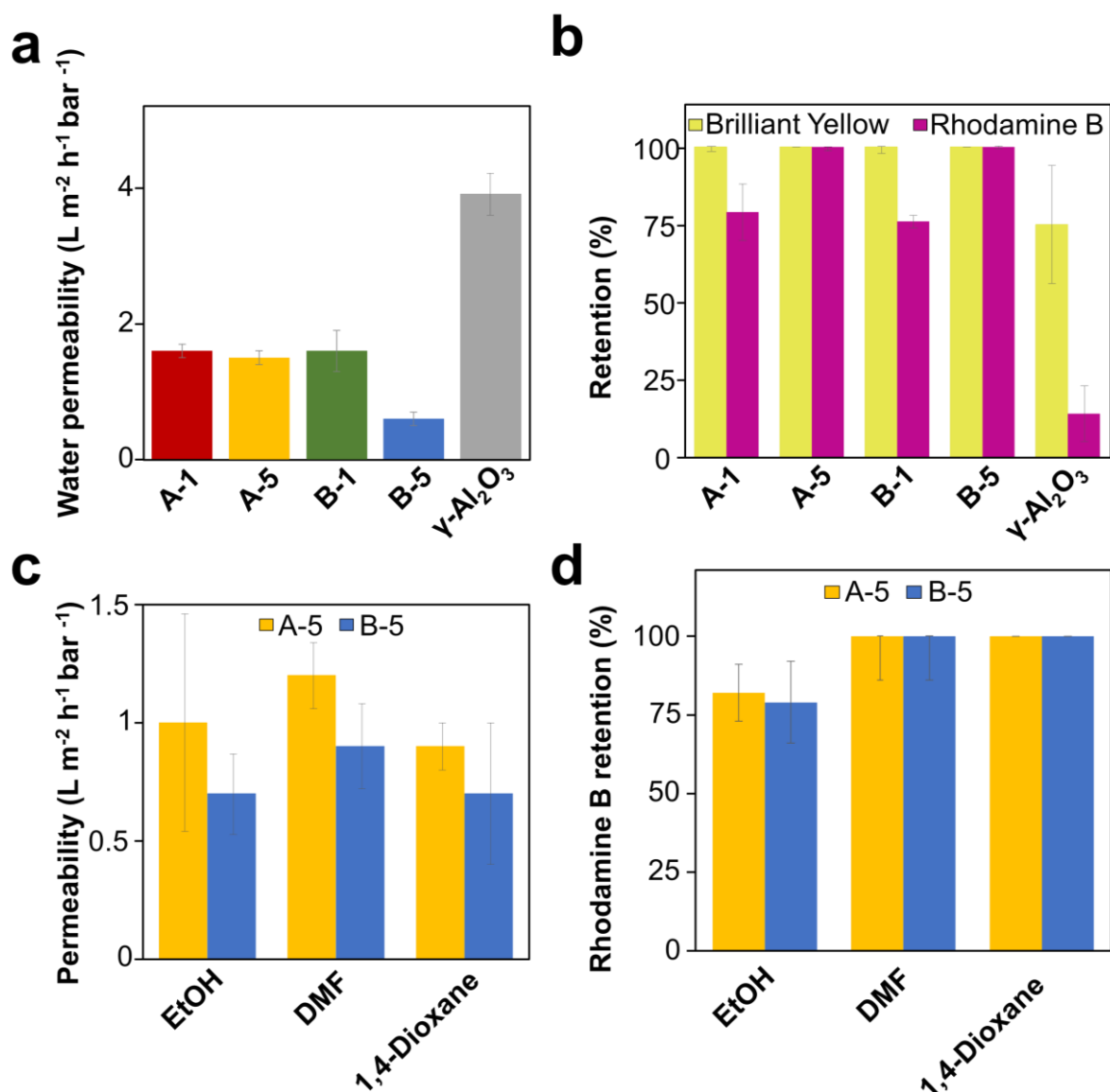


**Figure 4:** (a) Water permeability of the PI nanoconfined membranes and the pristine layer ( $\gamma$ -Al<sub>2</sub>O<sub>3</sub>). (b) Retention of Brilliant Yellow (BY) and Rhodamine B in water for PI nanoconfined membranes and the pristine layer ( $\gamma$ -Al<sub>2</sub>O<sub>3</sub>). Each test was repeated 3 times (the presented permeation and retention is an average and the errors refer to the standard deviation from the average value of 3 samples). (c) Performance of A-5 and B-5 samples in different solvents. (d) RB retention in different solvents for A-5 and B-5 samples.

The water permeability results, on the other hand, suggest a clear difference between route A and B, particularly for samples treated for 5 days. It is evidenced from the increase in RB

retention for sample A-5, compared to A-1 that for route A the polymer amount in  $\gamma$ -alumina pores is increasing and hence the pore is shrunk significantly. However, since the water permeability for A-5 remains comparable to that of A-1, this can be regarded as an indication that the polymer concentration is only increasing at the pore entrance, leading to thin selective barriers. For sample B-5, the RB retention is also increasing, compared to B-1, however here decreasing permeability is suggesting a thicker selective barrier. These preliminary results indicate that the polymer concentration is increasing with increasing reaction time (A-5 and B-5), but the location where the polymer concentration is increased depends on the pre-functionalization of the support. This means that for route A the polymer grows only at the top surface and pore entrance, positively influencing the retention of the membrane but leaving, evidently, unaffected the water permeability. On the other hand, for route B the polymer grows in the whole or part of the  $\gamma$ -alumina layer, as also indicated by EDS analysis. Hence, from this series of water permeation tests accompanied with permoporometry, HR-SEM and EDS analyses we have clearly evidenced that in the synthesis of PI nanoconfined membranes, the pre-functionalization step controls the extent of polymerization inside the mesoporous support.

Sample A-5 was also tested for 5 days in RB/water solution to assess the stability of the PI nanoconfined ceramic membranes. The results are provided in Figure S27. As shown, the RB retention remains stable at approximately 98-99%. Furthermore, the water flux increases slightly after the first day (from 8 to 10 L m<sup>-2</sup> h<sup>-1</sup>), but remains relatively stable in the following 4 days. Therefore, this preliminary result shows that the method used to prepare the PI nanoconfined membranes results in relatively stable membranes.

The two membranes showing the best rejection, the B-5 and A-5 samples, were subsequently tested in different solvents containing RB. The results for the solvent permeability and RB retention in solvents are given in Figure 4c and b, accordingly. Three

different organic solvents were selected based on their polarity; ethanol, DMF and 1,4-dioxane with polarity values of 0.654, 0.386, and 0.164 respectively. Indeed, by testing the membranes in different liquid media, we gain more insight into the membrane layer's properties. As shown in Figure 4c, the membranes perform well in all solvents. Only in ethanol, the retention performance of the PI nanoconfined membranes is lower than 90% (79% for B-5 and 83% for A-5). The results can be attributed to the nature and solubility of RB in different solvents. According to Hinckley et al.,<sup>41</sup> RB in a solution can be present in two forms, the lactone (L) and the zwitterionic (Z) form, which are in equilibrium, and the most dominant form depends on the solvent. Hinckley et al.<sup>41</sup> showed that the ratio zwitterionic:lactone (charged:neutral) in water (Z:L = 4.4) and formamide (Z:L = 7.67) is higher than in ethanol (Z:L = 2.4). Since ethanol favors the neutral form of RB, compared to water and DMF, we expect that the zwitterion rejection might be related to ionic repulsions between the membrane and the solute. Thus, leading to slightly lower rejections in ethanol.

In 1,4-dioxane, probably a different mechanism is at play. The solubility of RB in 1,4-dioxane is significantly lower than in ethanol, DMF or water. In this regard, the solvent is expected to have a much higher preference to the polymer (PI) than to the solute, leading to high retentions observed experimentally for the studied systems. These tests suggest that the PI network confined in the  $\gamma$ -alumina layer could be slightly charged since RB retentions are the best in water and DMF, where the zwitterionic form is dominant. The charge could originate either from the presence of primary terminal amines, which is also suggested from the FTIR analysis, and the monomer ratio used during membrane preparation. As such, we propose that by adjusting *in-situ* polymerization conditions, such as monomer ratio, one can tune the final membrane properties.

To conclude, a comparison between different membranes from literature with the A-5 membrane samples is shown in Figure 5. Evidently, A-5 is a potentially interesting membrane



with permeabilities in different solvents between 1 and 1.6 L m<sup>-2</sup> h<sup>-1</sup> bar<sup>-1</sup> and retentions in the NF range (469 g mol<sup>-1</sup>). However, since the water permeability of the pristine  $\gamma$ -alumina supported on  $\alpha$ -alumina (4 – 5 L m<sup>-2</sup> h<sup>-1</sup> bar<sup>-1</sup>) is relatively low, we expect that utilizing supports with thinner intermediate layer, for example of nanometer thickness, as well as an  $\alpha$ -alumina support with larger pore diameters and higher porosities can potentially improve the membrane performance even further.

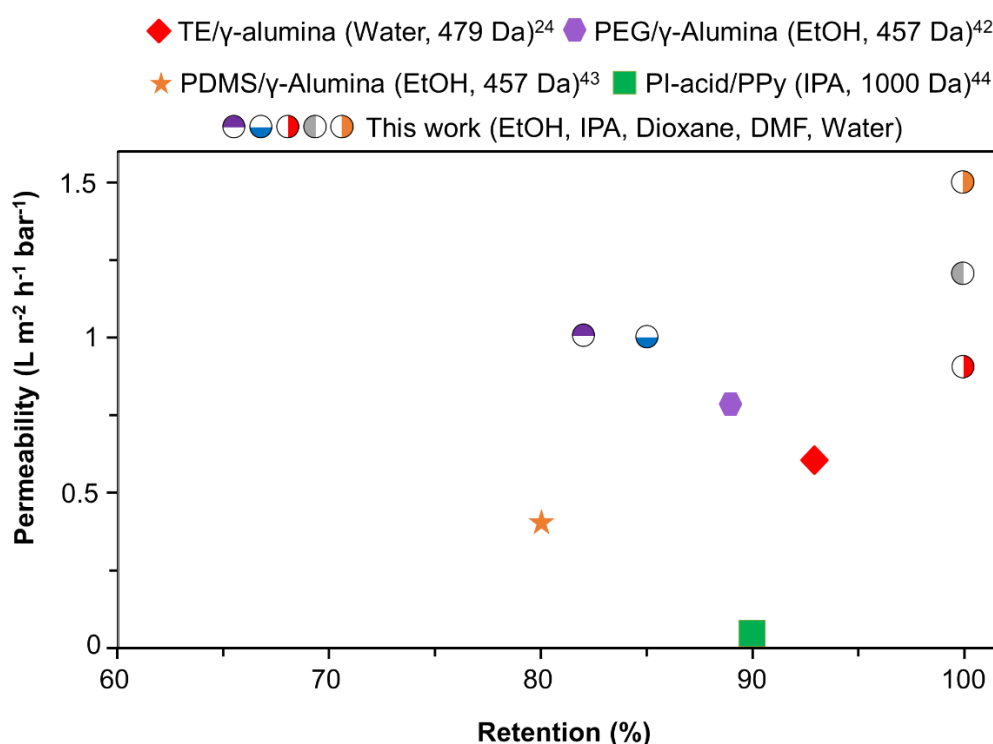


**Figure 5:** Comparison of the best performing membrane from this work (A-5) with other membranes reported in the literature (Solvents and Mw of dyes studied are given in brackets).<sup>24,42–44</sup> Membrane A-5 was tested in different solvents, including water, IPA, EtOH, DMF and dioxane, with RB (479 Da) as solute to ensure a good comparison with literature. The membranes used in this figure are similar in terms of the support or the membrane layer used.

## CONCLUSIONS

In this work, PI networks were confined in mesoporous inorganic layers by top or inner-pore surface-induced polyimidization. By pre-functionalizing of the top surface of the support, the polymeric network was confined at the top and entrance of the pores. Inner pore surface functionalization led to a homogeneous polymer distribution throughout the functionalized ceramic layer. The two monomers employed, MA and PMDA, allowed for forming a cross-linked and thus chemically resistant PI network inside the top layer of the ceramic support. By tuning the reaction time, we showed that the nanoconfinement of the polymer could also be effectively tuned. All these membranes were scrutinized through a series of characterization techniques, including SEM, FTIR, and pore diameter measurements, to demonstrate the influence of the applied methodology on their structure and final physicochemical properties. The as-prepared PI nanoconfined membranes showed attractive separation performance with good retentions of Rhodamine B ( $479 \text{ g mol}^{-1}$ ) in water and different organic solvents. At this moment, we do not foresee how to measure the resulting molecular weight that we expect to be very small, but this will be the object of further research using Molecular Dynamic simulation.

The principal asset of the work presented here relies on a demonstration of a method, allowing to control the polymerization of a cross-linked polymer inside the confined space of the 5.5 nm pores of the  $\gamma$ -alumina layer for the preparation of hybrid NF membranes. This work is a forerunner for confining polymers in nanoporous substrates and regulating the location of the polymer growth. We assume that this method can be used to grow polymers with even higher chemical resistance, such as polybenzimidazoles by using a similar preparation method as for polyimides. Furthermore, this method can be advantageously used as a tool in other fields to confine cross-linked polymers with low processability inside rigid supports to form for example low density, high strength, and thermal conductive nanocomposites for microelectronic insulation<sup>45–47</sup> or for anticorrosion coatings.<sup>48</sup>

## METHODS

**Materials.** Solvents ethanol (technical grade > 95%), anisole (>99%, Merck, NL), N-methyl-2-pyrrolidone (NMP) (>99%, anhydrous, Merck, NL), mesitylene (>99%, Acros Organics, NL), isoquinoline (95%, TCI, Europe), acetone (technical grade, > 95%), 1,4-dioxane (anhydrous, Sigma Aldrich, NL), dimethylformamide (> 99%, Sigma Aldrich, NL) and ethanol (analytical grade, Merck, NL) were used as received. Water was purified through a Milli-Q™ Reference Water Purification System. Glycerol (anhydrous, Merck, NL), 3-aminopropyl triethoxysilane (>98%, Sigma Aldrich, NL), pyromellitic dianhydride (PMDA) (97%, Sigma Aldrich, NL), melamine (MA) (99%, Sigma Aldrich, NL), Brilliant Yellow (70%, Sigma Aldrich, NL), Rhodamine B (> 99%, Merck, NL) were used as received. The chemical structures and abbreviations can be found in Figure S1 of the Supporting Information (SI).

**Support fabrication.** The  $\alpha$ -alumina ( $\alpha$ -Al<sub>2</sub>O<sub>3</sub> > 99 %) flat-sheet substrates (disc: diameter 21 mm, thickness 2 mm, 80 nm pore diameter) with one polished side were purchased from Pervatech B.V., the Netherlands. The polished side was dip-coated with a boehmite sol (prepared in-house) and subsequently calcined at 650 °C for 3 h to form a  $\gamma$ -alumina layer of 1.5  $\mu$ m in total thickness and 5.5 nm mean pore diameter. Further details for the fabrication of the  $\gamma$ -alumina layer can be found elsewhere.<sup>23,49</sup> The calcined supports were washed by immersion in a 2:1 v/v water/ethanol solution for at least 8h, at room temperature and then dried over-night, in a vacuum oven at 50 °C.

**Pre-functionalization of the top surface and pore entrance.** The  $\gamma$ -alumina layer was first filled with 1-2 mL of glycerol by rubbing the viscous liquid onto the surface and letting it soak for > 10 min. The top surface of the substrate was dabbed clean with a fiber-less tissue. Then, 21  $\mu$ l of 3-aminopropyl trimethoxysilane (APTES) was dissolved in anisole

(anhydrous) and transferred into a reaction vessel with the glycerol filled  $\gamma$ -alumina layer suspended above the solution. The solution was heated to 105 °C for 3h in a sealed vessel. After grafting, the functionalized porous support was washed with 20 mL anisole for 1h and 20 ml of water for 20 min under sonication and dried overnight at 50°C under vacuum. Amino-functionalized supports, obtained at this stage, were denoted as A.

**Pre-functionalization of the  $\gamma$ -alumina layer's inner pore surface.** Under inert atmosphere in a 50 mL reaction vessel charged with 40 mg (0.18 mmol) of PMDA, 20 mL of mesitylene were added and stirred for 1-2 min. A sample was then immersed in the solution and the mixture was heated to 160 °C over-night. The mixture was cooled to room temperature and the sample was washed with n-methyl-2-pyrrolidone (NMP) and acetone in a sonicated bath for 30 min. Finally, the sample (denoted as B) was dried in a vacuum oven at 50 °C over-night.

**Pore surface-induced polyimidization reaction.** In a 50 mL reaction vessel 530 mg (2.43 mmol) of PMDA and 260 mg (2.06 mmol) MA were added. Under inert atmosphere 9 mL of anhydrous NMP, 9 mL of mesitylene and 0.9 mL of isoquinoline were added in the reaction vessel and stirred for few minutes. Afterwards, the pre-functionalized sample (A or B) was added in the mixture and was heated to 200 °C for either 1 or 5 days. After the reaction was completed, the dark brown mixture was cooled to room temperature, and the membrane was removed from the solution and washed with 20 mL of NMP in a sonicated bath for 1h. Then, the membrane was immersed in 20 mL of fresh NMP and left for 3 days at room temperature to remove unreacted monomers or ungrafted polymer. Finally, the membrane was sonicated in 20 mL of acetone and dried in a vacuum oven at 50 °C over-night. Membrane samples prepared *via* route A (Scheme 1) are denoted as A-1 and A-5 (or A-1/5) respectively for 1 and 5 days of reaction. Samples prepared *via* route B (Scheme 1) are denoted as B-1 and B-5 (or B-1/5).

After the preparation of each membrane, the remaining reaction solution was collected and filtered under vacuum to yield a dark brown powder. These powders were then washed with 50 mL of NMP and 50 mL of acetone. Finally, the powders were dried in a vacuum oven at 50 °C over-night. Powder samples collected from the solution are denoted as I-1 and I-5. Detailed information on the spectroscopic characterization of the PI powders can be found in the SI.

**Material Characterization.** Fourier Transform Infrared spectroscopy (FTIR) measurements on both membrane and powder samples were done using a Perkin Elmer UATR Spectrum Two. Wavenumbers between 4000 and 550  $\text{cm}^{-1}$  were scanned in reflectance mode at a resolution of 4  $\text{cm}^{-1}$  for a minimum of 16 scans. Powder X-ray diffraction (XRD) patterns were recorded using a PANalytical X'Pert PRO diffractometer at the wavelength of Cu  $K\alpha$  ( $\lambda = 1.5405 \text{ \AA}$ ) (X-ray power: 40 kV, 40 mA) in Bragg-Brentano scanning mode. The program scanned angles ( $2\theta$ ) from 5 to 55 ° with a 0.026° step and a step time of 158s. Scanning electron microscopy (SEM) images of powder and membrane samples and energy-dispersive X-ray spectroscopy (EDS) were obtained using a JEOL JSM-6010LA scanning electron microscope using an accelerating voltage of 5 kV. SEM samples were sputtered with 5 nm of palladium/platinum layer to avoid sample charging. High resolution scanning electron microscopy (HR-SEM) micrographs of membrane samples were obtained with a Hitachi S-4800 field-emission scanning electron microscope (Japan) using an accelerating voltage of 2 kV. Samples were metallized with platinum to favor charge release. The change in pore diameter of the membrane samples was determined by permoporometry using cyclohexane as condensable vapor. The experimental procedure is described in detail elsewhere.<sup>46</sup> Water contact angles were measured using the sessile drop method, with 2  $\mu\text{L}$  drops of Milli-Q water. Atomic force microscopy (AFM) imaging was carried out in

intermittent-contact mode in air with AFM instrument Bruker Dimension ICON. The average roughness profile of the samples was determined by imaging  $1\ \mu\text{m}^2$  of each sample.

**Membrane performance.** Permeability and retention data were collected with a custom-made, dead-end filtration setup, connected *via* a pressure regulator valve to a nitrogen tank for pressurizing the solutions. Permeability ( $\text{L m}^{-2} \text{h}^{-1} \text{bar}^{-1}$ ) is expressed as the flux ( $\text{L h}^{-1}$ ) of water or a solvent across a membrane per unit of driving force, per square meter of exposed membrane area ( $2.4\ \text{cm}^2$ ). Flux data were collected by weighing the mass of permeate at four-time intervals, while permeability was determined from flux data at three applied transmembrane pressures between 8 and 20 bar, by taking the slope of a linear fit of the collected flux data. All slopes were found to be linear unless otherwise noted. Retentions ( $R$ ) of Brilliant Yellow (BY,  $M_w = 624.55\ \text{g mol}^{-1}$ , 50 ppm), Rhodamine B (RB,  $M_w = 479.02\ \text{g mol}^{-1}$ , 50 ppm) were calculated with the equation:

$$R = 1 - c_p/c_f \quad (1)$$

where  $c_p$  and  $c_f$  are the permeate and feed solute concentrations, respectively. Retention samples were obtained at recoveries between 35 and 50%. The dye adsorption during retention measurements was calculated with equation:

$$M_{Ads} = M_f - M_R + M_p \quad (2)$$

where,  $M_{Ads}$  is the amount of dye adsorbed on each membrane,  $M_f$  is the total amount of dye used at the beginning of each separation test (feed solution),  $M_R$  is the amount of dye in the retentate and  $M_p$  is the amount of dye in the permeate. In all cases, the dye concentration of BY and RB was increased in the retentate to account for limited adsorption of 2 – 3% for the PI nanoconfined ceramic membranes. Solute concentrations of BY and RB were calculated from Perkin-Elmer  $\lambda 12$  UV-Vis spectrophotometer results at the characteristic

wavelength of 401.5 (BY), 543 (RB/water), 554 (RB/water and RB/1,4-dioxane) and 560 (RB/DMF) nm.

## ASSOCIATED CONTENT

### Supporting Information

Chemical structures of compounds used; Complete FTIR spectra of the starting compounds and synthesized samples; X-ray diffraction analysis data; Cyclohexane pore radius measurement of grafted samples; High resolution SEM images of pristine support; EDS raw data of synthesized membrane samples.

## AUTHOR INFORMATION

### Corresponding Author

**Marie-Alix Pizzoccaro-Zilamy** - Inorganic Membranes, MESA+ Institute for Nanotechnology, University of Twente, 7500 AE Enschede, The Netherlands; [orcid.org/0000-0003-2496-099X](https://orcid.org/0000-0003-2496-099X); Email: [m.d.pizzoccaro@utwente.nl](mailto:m.d.pizzoccaro@utwente.nl)

**Louis Winnubst** - Inorganic Membranes, MESA+ Institute for Nanotechnology, University of Twente, 7500 AE Enschede, The Netherlands; [orcid.org/0000-0003-0362-1585](https://orcid.org/0000-0003-0362-1585); Email: [a.j.a.winnubst@utwente.nl](mailto:a.j.a.winnubst@utwente.nl)

### Authors

**Nikos Kyriakou** - Inorganic Membranes, MESA+ Institute for Nanotechnology, University of Twente, 7500 AE Enschede, The Netherlands; [orcid.org/0000-0002-8268-675X](https://orcid.org/0000-0002-8268-675X); Email: [n.kyriakou@utwente.nl](mailto:n.kyriakou@utwente.nl)

**Martin Drobek** - Institut Européen des Membranes, UMR5635, CNRS-UM-ENSCM, Université de Montpellier (CC047), Place Eugène Bataillon, 34095 Montpellier Cedex 5, France ; [orcid.org/0000-0003-2679-282X](https://orcid.org/0000-0003-2679-282X); Email: [martin.drobek@umontpellier.fr](mailto:martin.drobek@umontpellier.fr)

**Sissi de Beer** - Sustainable Polymer Chemistry Group, Department of Molecules & Materials, MESA+ Institute for Nanotechnology, University of Twente, 7500 AE Enschede, The Netherlands; orcid.org/0000-0002-7208-6814 Email: s.j.a.debeer@utwente.nl

**Arian Nijmeijer** - Inorganic Membranes, MESA+ Institute for Nanotechnology, University of Twente, 7500 AE Enschede, The Netherlands; Email: arian.nijmeijer@shell.com

### **Author Contributions**

N.K. designed and performed the experiments, and wrote part of the paper; MA.P.Z. supervised the project, helped with understanding the results and wrote part of the paper. M.D. provided important feedback on the manuscript and the figures; S.B. provided feedback on the manuscript and figures; A.N. is head of the group and provided important feedback on the work; L.W. supervised the whole project with weekly feedback and provided detailed scientific input during the progress of the project.

### **Funding Sources**

This work is part of the research program entitled ‘Solvent Tolerant Nanofiltration and reverse osmosis membranes for the purification of industrial aqueous streams’ (STNF), which is taking place within the framework of the Institute for Sustainable Process Technology (ISPT, project no BL-20-12).

### **ACKNOWLEDGMENTS**

Özlem Kap from the Physic of Complex Fluids is acknowledged for the AFM analysis. Bernard Fraisse from the Institut Charles Gerhardt, Montpellier, France and Karin Nieuwenhuijzen from the Inorganic Material Science group at the University of Twente are acknowledged for XRD and capillary measurements, respectively. Our special thanks go also to Didier Cot from Institut Européen des Membranes in Montpellier, France for the SEM observations of the membrane samples.



## REFERENCES

- (1) Sholl, D. S.; Lively, R. P. Seven Chemical Separations to Change the World. *Nature*. Nature Publishing Group April 26, 2016, pp 435–437. <https://doi.org/10.1038/532435a>.
- (2) Marchetti, P.; Solomon, M. F. J.; Szekely, G.; Livingston, A. G. Molecular Separation with Organic Solvent Nanofiltration: A Critical Review. *Chem. Rev.* **2014**, *114*, 10735–10806. <https://doi.org/10.1021/cr500006j>.
- (3) Vandezande, P.; Gevers, L. E. M. M.; Vankelecom, I. F. J. J. Solvent Resistant Nanofiltration: Separating on a Molecular Level. *Chem. Soc. Rev.* **2008**, *37* (2), 365–405. <https://doi.org/10.1039/b610848m>.
- (4) Merlet, R. B.; Pizzoccaro-Zilamy, M. A.; Nijmeijer, A.; Winnubst, L. Hybrid Ceramic Membranes for Organic Solvent Nanofiltration: State-of-the-Art and Challenges. *Journal of Membrane Science*. Elsevier B.V. April 1, 2020, p 117839. <https://doi.org/10.1016/j.memsci.2020.117839>.
- (5) Darvishmanesh, S.; Van der Bruggen, B. Mass Transport through Nanostructured Membranes: Towards a Predictive Tool. *Membranes (Basel)*. **2016**, *6* (4). <https://doi.org/10.3390/membranes6040049>.
- (6) Volkov, A. V.; Parashchuk, V. V.; Stamatialis, D. F.; Khotimsky, V. S.; Volkov, V. V.; Wessling, M. High Permeable PTMSP/PAN Composite Membranes for Solvent Nanofiltration. *J. Memb. Sci.* **2009**, *333* (1–2), 88–93. <https://doi.org/10.1016/j.memsci.2009.01.050>.
- (7) Baumgartner, B.; Puchberger, M.; Unterlass, M. M. Towards a General Understanding of Hydrothermal Polymerization of Polyimides. *Polym. Chem.* **2015**, *6* (31), 5773–5781. <https://doi.org/10.1039/c5py00231a>.
- (8) Vanherck, K.; Koeckelberghs, G.; Vankelecom, I. F. J. Crosslinking Polyimides for Membrane Applications: A Review. *Prog. Polym. Sci.* **2013**, *38* (6), 874–896. <https://doi.org/10.1016/j.progpolymsci.2012.11.001>.
- (9) Product overview - PuraMem® Membranes for organic solvent nanofiltration (OSN) - Evonik Industries <https://www.membrane-separation.com/en/organic-solvent-nanofiltration-with-puramem-duramem/product-overview> (accessed Jun 9, 2021).
- (10) Cai, D.; Su, J.; Huang, M.; Liu, Y.; Wang, J.; Dai, L. Synthesis, Characterization and Hydrolytic Stability of Poly (Amic Acid) Ammonium Salt. *Polym. Degrad. Stab.* **2011**, *96* (12), 2174–2180. <https://doi.org/10.1016/J.POLYMDEGRADSTAB.2011.09.008>.
- (11) Morikawa, A.; Iyoku, Y.; Kakimoto, M.-A.; Imai, Y. O. *Preparation of a New Class of Polyimide-Silica Hybrid Films by Sol-Gel Process*; 1992; Vol. 24.
- (12) Kuttiani Ali, J.; Maher Chabib, C.; Abi Jaoude, M.; Alhseinat, E.; Teotia, S.; Patole, S.; Hussain Anjum, D.; Qattan, I. Enhanced Removal of Aqueous Phenol with Polyimide Ultrafiltration Membranes Embedded with Deep Eutectic Solvent-Coated Nanosilica. *Chem. Eng. J.* **2021**, *408* (December 2020), 128017. <https://doi.org/10.1016/j.cej.2020.128017>.
- (13) Wei, C.; Qiang, R.; Lin, L.; Gao, Y.; Ma, S.; Zhang, X.; Huang, X. Combining Three-Dimensional Water Channels and Ultra-Thin Skin Layer Enable High Flux and Stability of Loose Polyimide/SiO<sub>2</sub> Nanofiltration Membranes at Low Operating Pressure via One Step in-Situ Modification. *J. Memb. Sci.* **2021**, *623* (December 2020), 118944.

<https://doi.org/10.1016/j.memsci.2020.118944>.

- (14) Qiang, R.; Wei, C. J.; Lin, L.; Deng, X.; Zheng, T.; Wang, Q.; Gao, Y.; Zhang, Y. Bioinspired: A 3D Vertical Silicon Sponge-Inspired Construction of Organic-Inorganic Loose Mass Transfer Nanochannels for Enhancing Properties of Polyimide Nanofiltration Membranes. *Sep. Purif. Technol.* **2021**, *259* (October 2020), 118038. <https://doi.org/10.1016/j.seppur.2020.118038>.
- (15) Mueller, N. C.; Van der Bruggen, B.; Keuter, V.; Luis, P.; Melin, T.; Pronk, W.; Reisewitz, R.; Rickerby, D.; Rios, G. M.; Wennekes, W.; Nowack, B. Nanofiltration and Nanostructured Membranes—Should They Be Considered Nanotechnology or Not? *J. Hazard. Mater.* **2012**, *211–212*, 275–280. <https://doi.org/10.1016/J.JHAZMAT.2011.10.096>.
- (16) Isaacson, S. G.; Lioni, K.; Volksen, W.; Magbitang, T. P.; Matsuda, Y.; Dauskardt, R. H.; Dubois, G. Fundamental Limits of Material Toughening in Molecularly Confined Polymers. *Nat. Mater.* **2016**, *15* (3), 294–298. <https://doi.org/10.1038/nmat4475>.
- (17) Isaacson, S. G.; Fostvedt, J. I.; Koerner, H.; Baur, J. W.; Lioni, K.; Volksen, W.; Dubois, G.; Dauskardt, R. H. Synthesis of Polyimides in Molecular-Scale Confinement for Low-Density Hybrid Nanocomposites. *Nano Lett.* **2017**, *17* (11), 7040–7044. <https://doi.org/10.1021/acs.nanolett.7b03725>.
- (18) Liu, G.; Müller, A. J.; Wang, D. Confined Crystallization of Polymers within Nanopores. *Acc. Chem. Res.* **2021**, *54* (15), 3028–3038. <https://doi.org/10.1021/ACS.ACCOUNTS.1C00242>.
- (19) Pizzoccaro-Zilamy, M.-A.; Huiskes, C.; Keim, E. G.; Sluijter, S. N.; van Veen, H.; Nijmeijer, A.; Winnubst, L.; Luiten-Olieman, M. W. J. New Generation of Mesoporous Silica Membranes Prepared by a Stöber-Solution Pore-Growth Approach. *ACS Appl. Mater. Interfaces* **2019**, *11* (20), 18528–18539. <https://doi.org/10.1021/acsami.9b03526>.
- (20) Home - inopor – the cutting edge of nano-filtration <https://www.inopor.com/en/> (accessed Nov 19, 2021).
- (21) Pervaporation Membranes by Pervatech <https://pervaporation-membranes.com/> (accessed Nov 19, 2021).
- (22) Abedini, S.; Parvin, N.; Ashtari, P.; Jazi, F. S. Microstructure, Strength and CO<sub>2</sub> Separation Characteristics of  $\alpha$ -Alumina Supported  $\gamma$ -Alumina Thin Film Membrane. *Adv. Appl. Ceram.* **2013**, *112* (1), 17–22. <https://doi.org/10.1179/1743676112Y.00000000043>.
- (23) Uhlhorn, R. J. R.; Veld, M. H. B. J. H. I.; Keizer, K.; Burggraaf, A. J. Synthesis of Ceramic Membranes. *J. Mater. Sci.* **1992**, *27* (2), 527–537. <https://doi.org/10.1007/BF00543947>.
- (24) Kyriakou, N.; Merlet, R. B.; Willott, J. D.; Nijmeijer, A.; Winnubst, L.; Pizzoccaro-Zilamy, M.-A. New Method toward a Robust Covalently Attached Cross-Linked Nanofiltration Membrane. *ACS Appl. Mater. Interfaces* **2020**, *12* (42), 47948–47956. <https://doi.org/10.1021/acsami.0c13339>.
- (25) Kyriakou, N.; Pizzoccaro-Zilamy, M.-A.; Nijmeijer, A.; Luiten-Olieman, M.; Winnubst, L. Hydrolytic Stability of PEG-Grafted  $\gamma$ -Alumina Membranes: Alkoxysilane vs Phosphonic Acid Linking Groups. *Microporous Mesoporous Mater.* **2020**, *307*, 110516.

<https://doi.org/10.1016/j.micromeso.2020.110516>.

- (26) Tanardi, C. R.; Pinheiro, A. F. M.; Nijmeijer, A.; Winnubst, L. PDMS Grafting of Mesoporous  $\gamma$ -Alumina Membranes for Nanofiltration of Organic Solvents. *J. Memb. Sci.* **2014**, *469*, 471–477. <https://doi.org/10.1016/j.memsci.2014.07.010>.
- (27) Merlet, R.; Winnubst, L.; Nijmeijer, A.; Amirilargani, M.; Sudhölter, E. J. R.; Smet, L. C. P. M. de; Cob, S. S.; Vandezande, P.; Dorbec, M.; Sluijter, S.; Veen, H. van; VanDelft, Y.; Wienk, I.; Cuperus, P.; Behera, S.; Hartanto, Y.; Vankelecom, I. F. J.; Wit, P. de. Comparing the Performance of Organic Solvent Nanofiltration Membranes in Non-Polar Solvents. *Chemie Ing. Tech.* **2021**, *93* (9), 1389–1395. <https://doi.org/10.1002/CITE.202100032>.
- (28) Sun, C.; Zhou, F.; Shi, L.; Yu, B.; Gao, P.; Zhang, J.; Liu, W. Tribological Properties of Chemically Bonded Polyimide Films on Silicon with Polyglycidyl Methacrylate Brush as Adhesive Layer. *Appl. Surf. Sci.* **2006**, *253* (4), 1729–1735. <https://doi.org/10.1016/j.apsusc.2006.03.019>.
- (29) Amirilargani, M.; Merlet, R. B.; Chu, L.; Nijmeijer, A.; Winnubst, L.; de Smet, L. C. P. M.; Sudhölter, E. J. R. Molecular Separation Using Poly (Styrene-Co-Maleic Anhydride) Grafted to  $\gamma$ -Alumina: Surface versus Pore Modification. *J. Memb. Sci.* **2019**, *582*, 298–306. <https://doi.org/10.1016/J.MEMSCI.2019.04.013>.
- (30) Coates, J. Interpretation of Infrared Spectra, A Practical Approach. In *Encyclopedia of Analytical Chemistry*; John Wiley & Sons, Ltd: Chichester, UK, 2006. <https://doi.org/10.1002/9780470027318.a5606>.
- (31) Merlet, R. B.; Amirilargani, M.; de Smet, L. C. P. M.; Sudhölter, E. J. R.; Nijmeijer, A.; Winnubst, L. Growing to Shrink: Nano-Tunable Polystyrene Brushes inside 5 Nm Mesopores. *J. Memb. Sci.* **2019**, *572*, 632–640. <https://doi.org/10.1016/j.memsci.2018.11.058>.
- (32) Tena, A.; Marcos-Fernández, A.; Lozano, A. E.; de la Campa, J. G.; de Abajo, J.; Palacio, L.; Prádanos, P.; Hernández, A. Thermally Treated Copoly(Ether-Imide)s Made from Bpda and Alifatic plus Aromatic Diamines. GAS Separation Properties with Different Aromatic Diamines. *J. Memb. Sci.* **2012**, *387–388* (1), 54–65. <https://doi.org/10.1016/j.memsci.2011.10.008>.
- (33) Pinheiro, A. F. M.; Hoogendoorn, D.; Nijmeijer, A.; Winnubst, L. Development of a PDMS-Grafted Alumina Membrane and Its Evaluation as Solvent Resistant Nanofiltration Membrane. *J. Memb. Sci.* **2014**, *463*, 24–32. <https://doi.org/10.1016/J.MEMSCI.2014.03.050>.
- (34) Mircescu, N. E.; Oltean, M.; Chis, V.; Leopold, N. FTIR, FT-Raman, SERS and DFT Study on Melamine. *Vib. Spectrosc.* **2012**, *62*, 165–171. <https://doi.org/10.1016/j.vibspec.2012.04.008>.
- (35) Li, Z.; Zhou, J.; Xu, R.; Liu, S.; Wang, Y.; Li, P.; Wu, W.; Wu, M. Synthesis of Three Dimensional Extended Conjugated Polyimide and Application as Sodium-Ion Battery Anode. *Chem. Eng. J.* **2016**, *287*, 516–522. <https://doi.org/10.1016/j.cej.2015.11.063>.
- (36) Wang, Y.; Gao, Q.; You, Q.; Liao, G.; Xia, H.; Wang, D. Porous Polyimide Framework: A Novel Versatile Adsorbent for Highly Efficient Removals of Azo Dye and Antibiotic. *React. Funct. Polym.* **2016**, *103*, 9–16. <https://doi.org/10.1016/J.REACTFUNCTPOLYM.2016.04.004>.

- (37) Sadhasivam, B.; Muthusamy, S. Synthesis and Characterization of Optically Active Polyimides and Their Octa(Aminophenyl)Silsesquioxane Nanocomposites. *High Perform. Polym.* **2016**, *28* (5), 547–561. <https://doi.org/10.1177/0954008315591021>.
- (38) Kim, H.-J.; Nam, S.-M. *High Loading of Nanostructured Ceramics in Polymer Composite Thick Films by Aerosol Deposition*; 2012; Vol. 7. <https://doi.org/10.1186/1556-276X-7-92>.
- (39) Baumgartner, B.; Bojdys, M. J.; Unterlass, M. M. Geomimetics for Green Polymer Synthesis: Highly Ordered Polyimides via Hydrothermal Techniques †. *Polym. Chem.* **2014**, *5*, 3727–3938. <https://doi.org/10.1039/c4py00263f>.
- (40) Duan, H.; Lyu, P.; Liu, J.; Zhao, Y.; Xu, Y. Semiconducting Crystalline Two-Dimensional Polyimide Nanosheets with Superior Sodium Storage Properties. *ACS Nano* **2019**, *13*, 2473–2480. <https://doi.org/10.1021/acsnano.8b09416>.
- (41) Hinckley, D. A.; Seybold, P. G.; Borris, D. P. Solvatochromism and Thermochromism of Rhodamine Solutions. *Spectrochim. Acta Part A Mol. Spectrosc.* **1986**, *42* (6), 747–754. [https://doi.org/10.1016/0584-8539\(86\)80095-2](https://doi.org/10.1016/0584-8539(86)80095-2).
- (42) Tanardi, C. R.; Catana, R.; Barboiu, M.; Ayril, A.; Vankelecom, I. F. J.; Nijmeijer, A.; Winnubst, L. Polyethyleneglycol Grafting of  $\gamma$ -Alumina Membranes for Solvent Resistant Nanofiltration. *Microporous Mesoporous Mater.* **2016**, *229*, 106–116. <https://doi.org/10.1016/J.MICROMESO.2016.04.024>.
- (43) Tanardi, C. R.; Nijmeijer, A.; Winnubst, L. Coupled-PDMS Grafted Mesoporous  $\gamma$ -Alumina Membranes for Solvent Nanofiltration. *Sep. Purif. Technol.* **2016**, *169*, 223–229. <https://doi.org/10.1016/J.SEPPUR.2016.05.057>.
- (44) Li, X.; Vandezande, P.; Vankelecom, I. F. J. Polypyrrole Modified Solvent Resistant Nanofiltration Membranes. *J. Memb. Sci.* **2008**, *320* (1–2), 143–150. <https://doi.org/10.1016/j.memsci.2008.03.061>.
- (45) Zhou, Y.; Chen, Y.; Wang, H.; Wong, C. P. Creation of a Multilayer Aluminum Coating Structure Nanoparticle Polyimide Filler for Electronic Applications. *Mater. Lett.* **2014**, *119*, 64–67. <https://doi.org/10.1016/j.matlet.2014.01.009>.
- (46) Zhou, Y.; Bai, Y.; Yu, K.; Kang, Y.; Wang, H. Excellent Thermal Conductivity and Dielectric Properties of Polyimide Composites Filled with Silica Coated Self-Passivated Aluminum Fibers and Nanoparticles. *Appl. Phys. Lett.* **2013**, *102* (25), 252903. <https://doi.org/10.1063/1.4812653>.
- (47) Li, X.; Dong, G.; Liu, Z.; Zhang, X. Polyimide Aerogel Fibers with Superior Flame Resistance, Strength, Hydrophobicity, and Flexibility Made via a Universal Sol–Gel Confined Transition Strategy. *ACS Nano* **2021**, *15*, 4768. <https://doi.org/10.1021/acsnano.0c09391>.
- (48) Sezer Hicyilmaz, A.; Ayse, ; Bedeloglu, C. Applications of Polyimide Coatings: A Review. **2021**, *3*, 363. <https://doi.org/10.1007/s42452-021-04362-5>.
- (49) Cuperus, F. P.; Bargeman, D.; Smolders, C. A. Permporometry: The Determination of the Size Distribution of Active Pores in UF Membranes. *J. Memb. Sci.* **1992**, *71* (1–2), 57–67. [https://doi.org/10.1016/0376-7388\(92\)85006-5](https://doi.org/10.1016/0376-7388(92)85006-5).

## SYNOPSIS

### Nanoconfined Polyimide Network into mesopores

